

1 **VOLUME AND RECURRENCE OF SUBMARINE-FAN-BUILDING TURBIDITY**
2 **CURRENTS**

3

4 Zane R. Jobe¹, Nick Howes², Brian W. Romans³, and Jacob A. Covault⁴

5

6 ¹Department of Geology and Geological Engineering, Colorado School of Mines, Golden, CO
7 80401

8 ²MathWorks, Natick, MA 01760

9 ³Department of Geosciences, Virginia Polytechnic Institute, Blacksburg, VA 24060

10 ⁴Bureau of Economic Geology, Jackson School of Geosciences, The University of Texas at
11 Austin, TX 78758

12

13 **ABSTRACT**

14 Submarine fans are archives of Earth-surface processes and change, recording
15 information about the turbidity currents that construct and sculpt them. The volume and
16 recurrence of turbidity currents are of great interest for geohazard assessment, source-to-sink
17 modeling, and hydrocarbon reservoir characterization. Yet, such dynamics are poorly
18 constrained. This study integrates data from four Quaternary submarine fans to reconstruct the
19 volume and recurrence of the formative turbidity currents. Calculated event volumes vary over
20 four orders of magnitude (10^5 to 10^9 m³), whereas recurrence intervals vary less, from 50 to 650
21 years.

22 The calculated turbidity-current-event volume magnitudes appear to be related to slope
23 position and basin confinement. Intraslope-fan deposits have small event volumes ($\sim 10^6$ m³)

24 while ponded-fan deposits have very large event volumes (10^8 to 10^9 m³). Deposits in non-
25 ponded, base-of-slope environments have intermediate values (10^7 to 10^8 m³). Sediment bypass
26 in intraslope settings and flow trapping in ponded basins likely accounts for these differences.
27 There seems to be no clear relationship between event recurrence and basin confinement. Weak
28 scaling exists between event volume and source-area characteristics, but sediment storage in
29 fluvial and/or intraslope transfer zones likely complicates these relationships. The methodology
30 and results are also applied to reconstruct the time of deposition of ancient submarine-fan
31 deposits.

32 The volume and recurrence of submarine-fan-building turbidity currents form
33 intermediate values between values measured in submarine canyons and channels ($<10^5$ m³ and
34 $<10^1$ yr) and on abyssal plains ($>10^8$ m³ and $>10^3$ yr), indicating that small, frequent flows
35 originating in submarine canyons often die out prior to reaching the fan, while rare and very
36 large flows mostly bypass the fan and deposit sediment on the abyssal plain. This partitioning of
37 flow volume and recurrence along the submarine sediment-routing system provides valuable
38 insights for better constraining geohazards, hydrocarbon resources, and the completeness of the
39 stratigraphic record.

40

41 **INTRODUCTION**

42 Turbidity currents carry sand and mud into the deep sea and create submarine fans, the
43 largest sediment accumulations on Earth (Talling *et al.*, 2015). Submarine fans are important
44 depositional archives of climate change (Gulick *et al.*, 2015; Bernhardt *et al.*, 2017), sea-level
45 fluctuations (Castelltort *et al.*, 2017), rates of continental erosion (Clift, 2006), land-to-sea
46 delivery of organic carbon (Burdige, 2005), and continental-margin seismicity (Goldfinger,

47 2011). They also host significant hydrocarbon resources (Pettingill & Weimer, 2002). Submarine
48 fans exhibit radial or cone-like morphologies in plan view and are composite features, consisting
49 of channel (with or without external levees) and lobe deposits (Shepard & Emery, 1941; Dill *et*
50 *al.*, 1954; Menard, 1955; Heezen *et al.*, 1959; Bouma *et al.*, 1985). Submarine fans form in net-
51 depositional environments of continental-margin sediment-routing systems, commonly
52 associated with slope breaks that promote sudden deceleration of turbidity currents and localized
53 deposition of sand beyond the slope break (Mutti & Normark, 1987; Adeogba *et al.*, 2005;
54 Spinewine *et al.*, 2009; Fernandez *et al.*, 2014; Jobe *et al.*, 2016; Picot *et al.*, 2016). The focus of
55 this paper is on the stratigraphic record of submarine fans, as their deposits likely contain a more
56 complete record of turbidity-current volume and recurrence (Piper & Normark, 1983) as
57 compared to channelized elements that are primarily conduits for turbidity-current bypass
58 (Hubbard *et al.*, 2014; Stevenson *et al.*, 2015).

59 The volume and recurrence of submarine-fan-building turbidity currents are of interest
60 for the assessment of geohazards, including tsunami hazards (Bondevik *et al.*, 1997; Goldfinger,
61 2011) and damage to submarine infrastructure (Carter *et al.*, 2012; Cooper *et al.*, 2013), inputs
62 for numerical models of sediment-routing systems (Petit *et al.*, 2015; Bolla Pittaluga & Imran,
63 2014; Sylvester *et al.*, 2015), and characterization of subsurface hydrocarbon resources (Saller *et*
64 *al.*, 2008). Studies utilizing outcrops, modern systems, and physical experiments provide insight
65 into the stratigraphic architecture and morphodynamics of submarine channel-fan depositional
66 systems (Normark, 1970; Pirmez *et al.*, 1997; Hodgson *et al.*, 2006; Sequeiros *et al.*, 2010;
67 Hubbard *et al.*, 2014; Cartigny *et al.*, 2013; de Leeuw *et al.*, 2016). Direct monitoring in modern
68 systems provides insight into the short-term morphodynamic and sediment-transport mechanisms
69 (Paull *et al.*, 2010; Cooper *et al.*, 2013; Hughes-Clarke, 2016; Clare *et al.*, 2016). However,

70 understanding the longer-term ($>10^2$ yr) recurrence of turbidity currents and the stratigraphic
71 evolution of submarine fans remains elusive (Talling *et al.*, 2015). In particular, few estimates of
72 sediment volume and recurrence of Holocene fan-building flows have been attempted, and the
73 few calculated volumes to date range seven orders of magnitude, from 10^{-5} to 10^2 km³ (Piper &
74 Aksu, 1987; Gonzalez-Yajimovich *et al.*, 2007; Clare *et al.*, 2016). Event recurrence is better
75 constrained, with Quaternary core-based studies providing recurrence interval data from multiple
76 basins (Clare *et al.*, 2014, 2016). Studies have also focused on the distribution of event
77 recurrence and how allogenic forcing and position along the sediment-routing system can affect
78 the recurrence distribution (Clare *et al.*, 2015; Allin *et al.*, 2016, 2017).

79 This study integrates seismic-reflection and core datasets from Quaternary submarine
80 fans to reconstruct the volume and recurrence of turbidity currents using simple parameters from
81 their deposits. This study focus on the following fans: 1) the Golo fan system, Corsica (Deptuck
82 *et al.*, 2008; Sømme *et al.*, 2011; Calvès *et al.*, 2012), 2) the 'X' intraslope fan, Nigeria (Pirmez
83 *et al.*, 2000; Prather *et al.*, 2012a; Jobe *et al.*, 2016), 3) the Brazos-Trinity intraslope fan system,
84 Texas (Beaubouef & Friedmann, 2000; Mallarino *et al.*, 2006; Pirmez *et al.*, 2012; Prather *et al.*,
85 2012b), and 4) the Hueneme fan, California (Gorsline, 1996; Normark *et al.*, 1998; Romans *et*
86 *al.*, 2009). Using the calculated ranges of event volume and recurrence, we estimate the time of
87 fan deposition in ancient submarine-fan successions, which commonly have poor age-
88 constraints. Finally, we discuss possible linkages between event volume and recurrence with 1)
89 source-area characteristics and 2) basin confinement and slope position.

90

91 **ESTIMATION OF TURBIDITY CURRENT VOLUME AND RECURRENCE**

92 This study presents a simple formulation that can be used to estimate sediment supply to
93 submarine fans in areas where data are sparse. While more sophisticated sediment mass balance
94 formulations exist (Paola & Voller, 2005 for short-term (sec) bed evolution), such calculations
95 require measurement of sediment concentration and flow velocity, which are very difficult to
96 obtain (Xu *et al.*, 2014; Talling *et al.*, 2015). The approach utilized here relies on three basic
97 measurements of submarine-fan deposits from seismic-reflection and core data (Fig. 1): 1) total
98 sediment volume V (m^3), (2) total duration of deposition T (yr), and (3) event count n . The
99 sediment volume V of a deposit was determined from seismic-reflection data using thickness of
100 mapped seismic-reflection horizons. When not provided by the original study, the bulk volume
101 was converted to sediment volume using reported porosity values using the equation bulk
102 volume*(1-porosity) = sediment volume. The total duration of deposition T was calculated using
103 chronologic information correlated between core data along seismic-reflection horizons that
104 bound submarine-fan deposits. Finally, the event count n is the number of turbidity-current
105 deposits in the volume V , and was determined from core data (Fig. 1). The event count is simply
106 the number of sand beds present in a core (Fig. 3). Where possible, amalgamated beds are
107 identified (core ‘fan 14 3 inch’ in Figure 3), but it is possible that some amalgamated beds are
108 unaccounted in the event count n . There is no interpreted hemipelagic sediment in the cores (cf.
109 Talling *et al.*, 2007a), and so we assume that the cores are composed entirely of turbidites and do
110 not include appreciable hemipelagic sediment. We also assume that there has been no post-
111 depositional erosion, reworking, or mass wasting. However, we recognize that these processes
112 occur, even in distal parts of submarine fans (Dennielou *et al.*, 2017; Croguennec *et al.*, 2017).
113 While we appreciate that event-bed geometries in submarine-fan deposits can be more complex
114 (Deptuck *et al.*, 2008; Jobe *et al.*, 2016), we also assume that core data accurately record the

115 event count n and that all events spread evenly across the fan/lobe. Where possible, an attempt is
116 made to define ranges of V , T , and n from multiple datasets to better encapsulate measurement
117 uncertainty and possible sampling bias from non-uniform deposition and the aforementioned
118 assumptions. Reasoning may suggest to only include the highest value of n as it samples the true
119 event count (Fig. 3), but we conservatively include the range derived from multiple cores where
120 possible because basin setting or other local factors may affect the spatial distribution of events.

121 The recurrence interval r (yr) is defined as the total time T divided by the event count n
122 (Eq. 1a). Turbidity-current frequency f (yr⁻¹) has the inverse relationship (Eq. 1b):

$$123 \quad r = \frac{T}{n} \text{ (Eq. 1a); } f = \frac{1}{r} \text{ (Eq. 1b)}$$

124 The average sediment volume deposited during a turbidity-current event (v_e) is related to
125 the total volume of a sediment package V (m³) and the number of events (n):

$$126 \quad v_e = \frac{V}{n} \text{ (Eq. 2)}$$

127 These relationships can be combined into an equation that equates the long-term deposition rate
128 and the average event volume and event recurrence (Eq. 3).

$$129 \quad \frac{V}{T} = \frac{v_e}{r} = v_e f \text{ (Eq. 3)}$$

130 It is important to note that v_e is an *average* event volume, and does not take into account the
131 distribution of flow volumes shown in natural systems (Talling *et al.*, 2007a; Cooper *et al.*, 2013;
132 Clare *et al.*, 2014; Allin *et al.*, 2017) and the spatial distribution of beds on a submarine fan
133 (Deptuck *et al.*, 2008; Jobe *et al.*, 2016). However, not enough detail about these distributions
134 are available to model them properly. Other assumptions about v_e include: 1) all sediment in an
135 individual turbidity current is deposited on the fan (Lamb *et al.*, 2004; Sylvester *et al.*, 2015) and
136 no deposition occurs in the canyon-channel system; 2) there is zero bypass to down-system sites;
137 3) there is no erosional bulking of the flows during transport; 4) there is no temporal change in v_e

138 during fan/lobe/feeder channel evolution (cf. Deptuck *et al.*, 2008; Clare *et al.*, 2016). While
139 these assumptions sometimes oversimplify the complexity of submarine-fan depositional
140 systems, they provide a general framework for estimating event volume (v_e) and recurrence (r)
141 for systems with limited data.

142

143 **STUDY LOCATIONS**

144 This study focuses on late Quaternary (< 130 ka) submarine-fan deposits, which are
145 suitable for determining V , T , and n due to high-quality seismic-reflection data and age-
146 constrained core data. The locales in this study occupy intraslope and base-of-slope settings (Fig.
147 2, Table 1).

148 **Niger X fan system, Nigeria**

149 Mobile shale deformation of the Niger continental slope (Pirmez *et al.*, 2000) created
150 intraslope accommodation where the Niger X submarine fan system was deposited. Jobe *et al.*
151 (2016) described late Quaternary deposits on the X fan and constrained V , T , and n of the
152 youngest sediment package (Fig. 2; Fig. 3; Table 2). The range of V is derived from the deposit
153 area and thickness measurements from cores (Table 2). The range of n is obtained by counting
154 event beds from two core descriptions (Fig. 3). The range of T is provided by adding/subtracting
155 the analytical error from radiocarbon ages to the value provided by Jobe *et al.* (2016). Prather *et*
156 *al.* (2012a) also measured values of V for longer term (> 100 kyr), thicker (>100 m) deposits on
157 the X fan, but these deposits are not included in our calculations because core data are lacking to
158 constrain T and n .

159 **Hueneme Fan system, California**

160 The Hueneme submarine fan developed in the Santa Monica Basin, offshore California
161 Continental Borderland (Fig. 2). The Quaternary fill of the Hueneme fan is ponded due to faults
162 and folds associated with transpressional deformation related to the San Andreas Fault system
163 (Piper & Normark, 2001; Normark *et al.*, 2006). Romans *et al.* (2009) measured V for five
164 intervals defined from seismic-reflection profiles that covered the entire Hueneme fan system,
165 and calculated T using radiocarbon ages from a core collected by Ocean Drilling Program (Site
166 1015; Table 2). The five intervals are grouped into three packages (Hueneme 1, 2, and 3-4-5,
167 following nomenclature of Romans *et al.*, 2009) that have values of $n > 2$ (for statistical
168 purposes) and approximately equal volume and time duration (Table 2). Ranges of n are
169 dependent on including or not including thin silt intervals and debris flow deposits, and
170 minimum and maximum values are presented based on this criterion (Table 2). The youngest
171 package (Hueneme 3-4-5) includes T and n values estimated by Gorsline (1996) from box cores
172 taken in a more proximal position. While some of the small, frequent flows discussed by
173 Gorsline (1996) may die out prior to reaching the Hueneme fan, these data are included as a
174 conservative approach to defining the parameter space of v_e and r .

175 **Brazos-Trinity system, Gulf of Mexico**

176 There are four linked intraslope salt-withdrawal basins in the Brazos-Trinity system that
177 contain Quaternary submarine-fan deposits (Winker, 1996; Badalini *et al.*, 2000; Beaubouef &
178 Friedmann, 2000; Mallarino *et al.*, 2006). Prather *et al.* (2012b) used 3D seismic-reflection data
179 to map the basin stratigraphy and demonstrate coeval deposition of three packages of sediment in
180 basins II and IV (40 series, 50/60 series, and 70 series in Table 2). Pirmez *et al.* (2012) used
181 borehole and core chronostratigraphy to calculate a sediment budget for the system, estimating V
182 and T for the three packages. Ranges of T were derived from minimum and maximum estimates

183 (Pirmez *et al.*, 2012). Ranges of n (Table 2) were derived for each package from the International
184 Ocean Discovery Program Site U1320 core description (fig. 4 of Pirmez *et al.*, 2012) in a similar
185 manner to that described for the Hueneme fan (above).

186 **Golo fan system, Corsica**

187 The comparatively small (cf. Sømme *et al.*, 2009) Golo submarine-fan deposits can be
188 entirely mapped on seismic-reflection profiles and exhibit base-of-slope fan architecture
189 (Deptuck *et al.*, 2008). Values of V and T were derived from Sømme *et al.* (2011) for Holocene
190 deposits (horizon K to seafloor) and from Calvès *et al.* (2012) for late Quaternary units S1, S2,
191 and S3 and also a Holocene fan package that occupies an intraslope position (the 'Pineto lobe' of
192 Deptuck *et al.*, 2008). Values of n were derived from two cores in Golo submarine-fan deposits
193 (Gervais, 2002; Gervais *et al.*, 2006). The cores used (kco62, kco58 upper section, and kco58
194 lower section) yield n values of 12, 6, and 8, respectively (figs 10 and 14 of Gervais *et al.*, 2006).
195 These cores are shallow piston cores and do not penetrate the entire intervals of interest; thus, n
196 values for each interval were extrapolated from these core data assuming no temporal change in
197 event recurrence. These extrapolated values of n (Table 2) are most appropriate for the youngest
198 deposits, but are also used for the older deposits, acknowledging that there may be temporal
199 changes in event recurrence that are not sampled by existing core data.

200

201 **DATA ANALYSIS**

202 Using measured values of V , T , and n from each locale, the methodology described above
203 can be used to estimate ranges of event volume and recurrence. Table 2 presents the values of V ,
204 T , and n measured from each studied locale. In all four study locales, ranges are often reported
205 for V , T , and n due to measurement uncertainty (e.g., measurement error in ages of Fig. 1) or

206 multiple possible values (Table 2). The Niger X fan is used as an example to explain the
207 measurements and uncertainties of V , T , and n . The sediment volume V was calculated using the
208 area of the youngest sediment package and the minimum and maximum thickness measurements
209 of 1 and 3 m based on core penetrations (Fig. 3; Jobe *et al.*, 2016). No areal changes in thickness
210 were assumed, rather a simple area*thickness was used to calculate minimum ($1.2 \times 10^7 \text{ m}^3$) and
211 maximum ($3.6 \times 10^7 \text{ m}^3$) values of V . The total duration of deposition T was determined from
212 core-derived radiocarbon ages (fig. 9 of Jobe *et al.*, 2016) and is estimated to be $4,000 \pm 200 \text{ yr}$
213 (Fig. 3). The event count n was obtained by counting the sand beds in two core descriptions
214 ($n=20$, $n=48$; Fig. 3; Table 2).

215 In order to fully explore the parameter space for v_e and r , the ranges of the input values V ,
216 T , and n are determined by using a uniform distribution (Table 2). To create a uniform
217 distribution of each variable (V , T , n), the range between the minimum and maximum values is
218 divided into 10,000 values. Using random sampling with replacement, r and v_e are calculated
219 10,000 times using Equations 1a and 2, respectively. The 10,000 iterations of v_e and r for the
220 Niger X fan can be plotted as a ‘size-recurrence’ plot (Fig. 4A).

221 A triangular distribution is employed which approximates a normal distribution in cases
222 of limited data. For each variable (V , T , n), the minimum value, maximum value, and the mean
223 of those two values are used to define the lower limit, upper limit, and peak location of the
224 triangular distribution. Using random sampling with replacement, v_e and r are again calculated
225 10,000 times, with the results displayed in an event volume-recurrence plot (Fig. 4B). A 2D
226 kernel density emphasizes the resulting distribution of v_e and r , with the kernel shown as a
227 contour map containing 90% of the data (Fig. 4B). Calculating v_e and r from uniform
228 distributions of V , T and n results in the largest, most conservative parameter space (Fig. 4A).

229 Using a triangular distribution slightly shrinks the overall distribution of the parameter space but
230 does not significantly alter the results obtained with a uniform distribution (Fig. 4B).

231

232 **RESULTS**

233 For the four studied locales, values of v_e vary over four orders of magnitude (10^5 - 10^9 m³),
234 while values of r vary by one order of magnitude (50-650 yr, Fig. 5). The intraslope deposits of
235 the Niger X and Golo Pineto locales show the smallest values of v_e , approximately 10^6 m³ (Fig.
236 5). The base-of-slope Golo deposits have intermediate v_e values (10^7 m³, Fig. 5). The ponded
237 Brazos-Trinity and Hueneme deposits have the largest values of v_e ($>10^8$ m³) and the most
238 variability in r (Fig. 5). Interestingly, the three time intervals in the Brazos-Trinity system have
239 quite different values of r but very consistent values of v_e . The Golo Pineto locale has the largest
240 variability in v_e and r of any deposit, likely due to the wide ranges of input values of T and n
241 (Table 2).

242 **Validation of the calculated values of v_e and r**

243 In order to ensure that the calculated values of v_e are reasonable, the distribution of event-
244 bed thickness in a submarine fan deposit can be estimated and compared to well-constrained
245 examples from outcrops and modern systems. For the Niger X fan, values of n (Table 2) and a
246 package thickness of 2 m (the average thickness estimate of Jobe *et al.*, 2016) are used to
247 estimate average event-bed thickness of 4.2 cm and 10 cm (for $n = 48$ and 20, respectively).
248 These thickness values are well within the observed range of event-bed thickness (1-57 cm,
249 average of 10 cm) for cores from the X fan (Jobe *et al.*, 2016) as well as other reported event-bed
250 thickness ranges (3-110 cm from Pr lat & Hodgson, 2013). These ranges of event-bed thickness

251 are also comparable to other well-characterized submarine-fan deposits (Murray *et al.*, 1996;
252 Talling, 2001; Sylvester, 2007; Prélat *et al.*, 2009).

253

254

255 **DISCUSSION**

256 **Estimating the total time of deposition (T) in ancient submarine fan deposits**

257 Ancient submarine-fan deposits are well described from subsurface data (Normark, 1970;
258 Saller *et al.*, 2008; Kane & Ponten, 2012) and outcrop exposures (Walker, 1978; Hodgson *et al.*,
259 2006; Pyles, 2008; Prélat *et al.*, 2009; Auchter *et al.*, 2016). Facies relationships and stratigraphic
260 architecture are mappable in outcrops and, with areally extensive exposures, volumes can be
261 estimated. However, the total time of deposition (T) and the event recurrence interval (r) are
262 difficult to determine accurately due to large uncertainties of chronostratigraphic methods for
263 sedimentary rocks. However, we can use estimated volumes (V) for outcropping submarine-fan
264 deposits and calculated ranges of r and v_e from Quaternary systems (Fig. 5) to estimate the total
265 time of deposition T for the ancient, outcropping deposits. These estimates of T can aid in the
266 interpretation of the incomplete and low-resolution geochronology typical of ancient submarine-
267 fan deposits.

268 Submarine-fan deposits containing six discrete sediment packages were mapped in the
269 Permian Skoorsteen Formation in the Tanqua Karoo sub-basin, South Africa by Prélat *et al.*
270 (2009). These six packages were classified hierarchically as ‘lobes’ by Prélat *et al.* (2009) and
271 the encompassing unit a ‘lobe complex’; however, we will refer to them generically as sediment
272 packages to avoid terminology confusion. These submarine-fan deposits are interpreted to have
273 formed in a base-of-slope position in an unconfined (i.e., non-ponded) basin (Prélat *et al.*, 2009),

274 most similar to the Golo locale (Table 1). The U-Pb ages from ashes interbedded with the
275 sediment packages of the Skoorsteenberg Formation are all within error of each other (Fildani *et*
276 *al.*, 2009) and may include erroneous ages due to magmatic crustal recycling during volcanic
277 eruptions (McKay *et al.*, 2015). Hence, it is not possible to accurately calculate T values from
278 these U-Pb ages; it is, however, possible to estimate ranges of T using the approach described
279 above. Prélat *et al.* (2009) calculated V for three of the mapped packages ('lobes' 2, 5, and 6),
280 with values of 1.3 to 3.5 x 10⁹ m³ (Table 3), similar to calculated sediment volumes from this
281 study (Table 2) and other Quaternary submarine-fan deposits (Prélat *et al.*, 2010). Using lobe
282 volume and event count data (Table 2), Equation 2 is used to define potential values of v_e for
283 lobes 2, 5 and 6, which are ~ 10⁸ m³ (Table 2). To be conservative, values of v_e that bracket these
284 estimates are chosen (10⁷ to 10⁹ m³), which are also most similar to other base-of-slope systems
285 (Fig. 5). The range of r is conservatively chosen as 50-650 yr, encompassing all of the data in
286 Figure 5. Uniform distributions of each variable are created as inputs into Equation 3 (using the
287 same methods as described above) to calculate a range of T for the three packages (Fig. 6). The
288 P₅₀ prediction of T for each package is on the order of 10⁴ yr (Fig. 6). Specifically, 'lobe' 2 has
289 T_{P50} =1.5 kyr, 'lobe' 5 has T_{P50} =2.5 kyr, and 'lobe' 6 has T_{P50} =0.9 kyr (Fig. 6). These lobe
290 duration estimates compare reasonably to the Holocene Amazon (15-20 lobes in 10 kyr, Jegou *et*
291 *al.*, 2008) and Zaire (38-52 lobes in 210 kyr, Picot *et al.*, 2016) submarine fan deposits (Fig. 6).
292 The hierarchically larger package ('lobe complex' of Prélat *et al.*, 2009 often informally referred
293 to as 'Fan 3') consists of six 'lobes'; if minimum and maximum values from Figure 6 are used to
294 estimate T for the lobe complex, the range of T for 'Fan 3' is 1.6-68 kyr, with median values
295 ranging from 5-15 kyr. This analysis provides a methodology for estimating the total time of
296 deposition (T) for ancient submarine-fan successions where no other data are available. This

297 analysis also highlights the need for more volumetric and geochronologic characterization of
298 ancient submarine-fan deposits.

299 **Linking catchment parameters to event volume**

300 Source (e.g., catchment dimensions) and sink (e.g., submarine-fan length) parameters
301 have been shown to generally scale to one another (Sømme *et al.*, 2009). The event volume
302 measured in the sink (Fig. 5) should scale to a sediment supply parameter (e.g., sediment load) in
303 the source area, given minimal storage in the transfer zone (Romans *et al.*, 2016). In order to
304 investigate these relationships, source parameters (Table 2) were compiled for the four systems
305 from Milliman and Farnsworth (2011), including catchment area (km²), sediment yield
306 (tons/km²/yr), and sediment load (tons/yr). For the Golo, Hueneme, and Brazos-Trinity systems a
307 weighted average was calculated for catchments that feed these systems (see Table 2), and for
308 the Niger system, one-quarter of the Niger river parameters were used, as Allen (1965) estimates
309 that the study area of the western Niger Delta receives approximately one-quarter of the water
310 and sediment discharge. Figure 7 plots catchment area, sediment yield, and sediment load against
311 the median value of event volume (v_e) calculated for each system, which show positive, but
312 weak, correlations between catchment parameters and event volume. The Niger forms a
313 consistent outlier to this dataset (Fig. 7), suggesting that sediment partitioning in the Niger Delta
314 may not be accurately estimated by Allen (1965); unfortunately, more detailed data are not
315 available. While these scaling relationships (Fig. 7) seem reasonable and corroborate other
316 source-to-sink scaling relationships (Sømme *et al.*, 2009), more systems are needed to further
317 test this hypothesis and derive any statistical significance.

318 The weak scaling shown in Figure 7 indicates poor connectivity between source and sink.
319 When comparing source parameters and event volume, we assume complete transfer of sediment

320 from the source to the sink, but many modern systems have significant sediment storage in the
321 fluvial transfer zone (Wilson & Goodbred, 2015; Romans *et al.*, 2016) that could complicate
322 scaling between catchment parameters and v_e . For example, the Niger X system may have
323 significant transfer-zone storage not accounted for by Allen (1965), and thus would plot far
324 below its current position in Fig. 7.

325 **Linking event volume to the basin setting of submarine fans**

326 While the values of r remain relatively consistent across all basin settings, the values of
327 v_e vary by orders of magnitude (Fig. 5). The studied submarine sediment-routing systems occupy
328 different tectonic and topographic basin settings (Table 1) that may control the values of v_e . (e.g.,
329 basin ponding, intraslope basin development). These different basin settings can lead to the
330 sequestration of sediment and thus a further decoupling of the source-to-sink scaling
331 relationships described above. For example, the calculated values of v_e for ponded basin floor
332 settings (the Brazos-Trinity and Hueneme systems) are much larger than for base-of-slope and
333 intraslope fans (Fig. 5). There is no sediment bypass in the Brazos Trinity and Hueneme systems
334 as compared to the intraslope X fan and Golo Pineto locales. The Brazos-Trinity system is fully
335 ponded by a large salt diapir at the distal edge of Basin IV (Prather *et al.*, 2012b; Pirmez *et al.*,
336 2012), and the Hueneme fan is ponded by various fault-related ridges and knolls (Normark *et al.*,
337 1998). On the intraslope Niger X fan, on the other hand, there is direct seafloor and core
338 evidence for sediment bypass in the form of an exit channel at the distal edge of the fan (Fig. 3;
339 Jobe *et al.*, 2016) and thus small values of v_e may be expected. The Golo Pineto deposit also
340 occupies an intraslope position (Deptuck *et al.*, 2008) and likely experienced sediment bypass
341 and thus smaller values of v_e . The larger Golo submarine fan deposits (Fig. 5) occupy a non-
342 ponded base-of-slope position, and thus show intermediate ranges of v_e .

343 **Comparison to other turbidity-current volumes and frequencies: from proximal submarine**
344 **canyons to abyssal plains**

345 This study focuses on event volumes and frequencies of turbidity currents that build
346 submarine fans. However, there is a full spectrum of event-based measurements from upslope
347 submarine canyons to downslope abyssal plains, measured using direct monitoring data as well
348 as core and outcrop data. These emerging datasets enable a comparison of event volumes and
349 recurrence intervals across the entire submarine sediment-routing system. It is important to note
350 that these trends are only valid for abyssal plains that are fed by the same feeder system as the
351 canyon/channel and fan (cf. Talling *et al.*, 2007b).

352 *Abyssal plains*

353 Abyssal plains have been recognized as a source for palaeoclimate (Clare *et al.*, 2015)
354 and palaeoearthquake (Goldfinger, 2011) records because they preserve a relatively complete
355 depositional record due to little or no erosion and/or post-depositional modification (Weaver *et*
356 *al.*, 1992). A large compilation by Clare *et al.* (2014) of turbidite volumes (v_e) and recurrence
357 intervals (r) for three abyssal plains allows us to assess the magnitude differences between
358 turbidity currents that build submarine fans and those that deposit sand in the most distal
359 locations on Earth. The data (Clare *et al.*, 2014) are derived from well-studied and dated cores
360 from the modern Madeira Abyssal Plain (offshore northwest Africa) and the modern Balearic
361 Abyssal Plain (western Mediterranean Sea), and also from outcrops of the Miocene Marnoso-
362 Arenacea Formation, Italy (Amy & Talling, 2006). Generally, values of v_e and r for turbidity
363 currents building submarine fans are 10-1,000 times smaller and 10-100 times more frequent
364 than turbidity currents depositing sand onto the abyssal plain (Fig. 8). This is an intuitive
365 relationship that was also recognized by Piper and Normark (1983). Large-volume turbidites on

366 abyssal plains can have many triggers, including large-magnitude earthquakes (Normark and
367 Piper, 1991; Piper and Normark, 2011), glacial advances (Haflidason *et al.*, 2004), sea-level
368 regressions (Kolla & Perlmutter, 1993), and sea-level transgressions (Hunt *et al.*, 2013).
369 However, Clare *et al.* (2014) find that some abyssal plain turbidites are temporally random and
370 not linked to sea level at all. Regardless of the mechanism, abyssal plain turbidites have 10-1,000
371 times larger event volumes than turbidity currents building submarine fans, but occur 10-100
372 times less frequently (Fig. 8). However, there is some overlap between the abyssal plain values
373 and large volume flows that characterize the ponded locales of the Hueneme and Brazos-Trinity
374 systems. The ponding in both these systems may result in larger calculated v_e values, as ponding
375 is an effective sediment-trapping mechanism.

376

377 *Proximal submarine canyons*

378 The heads of submarine canyons, at the other extremity of the submarine sediment
379 routing system, have been instrumented for decades (Prior *et al.*, 1987; Paull *et al.*, 2010), and
380 have served as natural laboratories that enable a better understanding of turbidity current
381 morphodynamics (Cooper *et al.*, 2013; Hughes-Clarke, 2016; Jobe *et al.*, 2017; Symons *et al.*,
382 2017). While event volumes have thus far eluded the flow monitoring datasets, recurrence
383 intervals spanning from hours (Hughes-Clarke, 2016) to years (Paull *et al.*, 2014) have been
384 documented. However, many of these flows, while very frequent, dissipate prior to reaching the
385 submarine fan (Paull *et al.*, 2005; Talling *et al.*, 2015) and thus must have relatively small event
386 volumes ($v_e < 10^5 \text{ m}^3$). Further evidence of frequent and small-volume flows not reaching
387 submarine fans comes from the Iberian abyssal plain (not discussed here, see Allin *et al.*, 2017)
388 and the Hueneme submarine fan. Romans *et al.* (2009) suggest that frequent, thin-bedded

389 turbidites with short recurrence intervals (Table 2) recovered in cores from the proximal
390 Hueneme canyon by Gorsline (1996) are not represented in the Hueneme submarine fan deposits,
391 indicating that these frequent, small magnitude flows dissipated prior to reaching the fan.

392 *Event volumes and frequencies across the submarine sediment-routing system*

393 The observations above are summarized in a generalized parameter space for event
394 volume and recurrence (Fig. 8) that is inspired by pioneering work on the size spectrum of
395 turbidity currents (Piper & Normark, 1983). The ranges of event volume and recurrence can be
396 classified into three overlapping categories: submarine canyon, submarine fan, and abyssal plain
397 (Fig. 8). This continuum of flow processes is reflected in the often-smooth geomorphic transition
398 from canyon to fan to basin plain (Piper & Normark, 2001). Small flows are generated in
399 submarine canyons very frequently, but few of those flows reach the submarine fan (Stevens *et*
400 *al.*, 2013; Clare *et al.*, 2016). Very large and infrequent flows deposit sediment onto the abyssal
401 plain, and likely partially bypass the submarine fan (Fig. 8). It seems that flows that build
402 submarine fans occupy an intermediate position in terms of event volume ($10^5 - 10^9 \text{ m}^3$) and
403 recurrence ($10^1 - 10^3 \text{ yr}$), where flow filtering through submarine canyons and channels
404 (McHargue *et al.*, 2011) and distance from source (Stevens *et al.*, 2013; Allin *et al.*, 2017)
405 probably play significant roles in modulating flow volume and recurrence to submarine fans.
406 Thus, fans are constructed by flows large enough to bypass and sculpt canyons, but small enough
407 to die out before reaching the abyssal plain. It is important to note that event volume and
408 recurrence are not single values, but rather distributions, and it is likely that these distributions
409 are truncated as flows move from canyon to basin plain (Allin *et al.*, 2017). As more data are
410 collected and analyzed, event volume and recurrence will become better understood and better
411 able to provide sediment flux estimates and assessments of submarine geohazards.

412

413 **CONCLUSIONS**

414 This study applies a simple mass-balance approach to four well-characterized Quaternary
415 submarine-fan deposits in order to calculate the volumes of sediment deposited by turbidity
416 currents and the recurrence of those events. The ranges of event volume vary over four orders of
417 magnitude, from 10^5 to 10^9 m³, while recurrence intervals vary by one order of magnitude, from
418 50 to 650 yr. These flow parameters seem to typify turbidity currents that build submarine fans,
419 and form intermediate values between events measured in submarine canyons and on abyssal
420 plains. Measured turbidity currents in submarine canyons have small volumes (less than 10^5 m³)
421 and short recurrence intervals (hours to years), while turbidites deposited on abyssal plains have
422 very large event volumes (greater than 10^8 m³) and long recurrence intervals (10^2 to 10^6 yr). The
423 segmentation of flow volume and recurrence along the submarine sediment-routing system
424 provides valuable insights for better constraining models for geohazard assessment and resource
425 characterization. Calculations of event volume and recurrence can also be used to estimate the
426 time of deposition in ancient submarine-fan successions where high-resolution chronologic data
427 are not available. Applying this methodology, to the well-known 'Fan 3' of the Tanqua Karoo
428 fan system (South Africa), we estimate the time of deposition of Fan 3 to be 5-15 kyr.

429 The volumes of submarine-fan-building turbidity currents calculated by this study show
430 correlations to slope position and topographic complexity, with ponded submarine fans having
431 larger event volumes than base-of-slope and intraslope fans. Non-ponded intraslope submarine
432 fans have smaller event volumes than ponded or base-of-slope submarine fans, likely because of
433 flow bypass (as opposed to flow trapping in ponded basins) and because only the largest flows
434 reach the basin floor/abyssal plain. There is weak positive scaling of event volume to source area

435 characteristics (e.g., catchment area, sediment yield), but submarine topographic complexity
436 (e.g., ponding, bypass) and sediment storage in the fluvial transfer zone potentially complicate
437 these scaling relationships. Further work should focus on improved volumetric and
438 geochronologic characterization of modern and ancient submarine fan deposits from a range of
439 sediment supply characteristics, source-to-sink configurations, tectonic settings, and geographic
440 locations to enable investigation of trends in event volume and recurrence and how various
441 system characteristics may influence deviations from norms.

442

443 **ACKNOWLEDGMENTS**

444 We acknowledge reviewers Mike Clare and Joris Eggenhuisen and associate editor
445 Matthieu Cartigny, whose careful and thoughtful reviews greatly enhanced the quality and
446 readability of this article. We also thank Matt Wolinsky, Oriol Falivene, John Martin, Ash
447 Harris, Morgan Sullivan, Hajime Naruse, Zoltan Sylvester, and Alessandro Cantelli for topical
448 discussions. ZRJ acknowledges support from Chevron through the Center of Research
449 Excellence (core.mines.edu), and JAC acknowledges support of the Quantitative Clastics
450 Laboratory sponsors (beg.utexas.edu/qcl).

451

452 **REFERENCES**

- 453 **Adeogba, A.A., McHargue, T.R. and Graham, S.A.**, 2005, Transient fan architecture and depositional controls
454 from near-surface 3-D seismic data, Niger Delta continental slope: AAPG Bulletin, v. 89, p. 627–643, doi:
455 10.1306/11200404025.
- 456 **Allen, J.R.L.**, 1965, Late Quaternary Niger delta, and adjacent areas: sedimentary environments and lithofacies:
457 AAPG Bulletin, v. 49, p. 547–600.
- 458 **Allin, J.R., Hunt, J.E., Talling, P.J., Clare, M.A., Pope, E. and Masson, D.G.**, 2016, Different frequencies and
459 triggers of canyon filling and flushing events in Nazaré Canyon, offshore Portugal: Marine Geology, v.

- 460 371, p. 89–105, doi: 10.1016/j.margeo.2015.11.005.
- 461 **Allin, J.R., Hunt, J.E., Clare, M.A. and Talling, P.J.**, 2017, Eustatic sea-level controls on the flushing of a shelf-
462 incising submarine canyon: *Geological Society of America Bulletin*, v. 130, p. 222–237, doi:
463 10.1130/B31658.1.
- 464 **Amy, L.A. and Talling, P.J.**, 2006, Anatomy of turbidites and linked debrites based on long distance (120 x 30 km)
465 bed correlation, Marnoso Arenacea Formation, Northern Apennines, Italy: *Sedimentology*, v. 53, p. 161–
466 212, doi: 10.1111/j.1365-3091.2005.00756.x.
- 467 **Auchter, N.C., Romans, B.W. and Hubbard, S.M.**, 2016, Influence of deposit architecture on intrastratal
468 deformation, slope deposits of Tres Pasos Formation, Chile: *Sedimentary Geology*, v. 341, p. 13-26, doi:
469 10.1016/j.sedgeo.2016.05.005.
- 470 **Badalini, G., Kneller, B. and Winker, C.D.**, 2000. Architecture and processes in the late Pleistocene Brazos-
471 Trinity turbidite system, Gulf of Mexico continental slope. In: Weimer, P., Slatt, R.M., Coleman, J., Rosen,
472 N.C., Nelson, H., Bouma, A.H., Styzen, M.J., Lawrence, D.T. (Eds.), *Deep-water Reservoirs of the World.*
473 *Proceedings of the 20th Annual Research Conference. Gulf Coast Section SEPM Foundation*, p. 16-34.
- 474 **Beaubouef, R.T. and Friedmann, S.J.**, 2000, High resolution seismic/sequence stratigraphic framework for the
475 evolution of Pleistocene intra slope basins, western Gulf of Mexico: depositional models and ... (N. C.
476 Rosen, P. Weimer, S. M. Coutes dos Anjos, S. Henrickson, E. Marques, M. Mayall, R. Fillon, T.
477 D'Agostino, A. Saller, K. Champion, T. Huang, R. Sarg, & F. Schroeder, Eds.): *Deep-Water Reservoirs of*
478 *the World.*, doi: 10.5724/gcs.12.32.
- 479 **Bernhardt, A., Schwanghart, W., Hebbeln, D., Stuut, J.-B.W. and Strecker, M.R.**, 2017, Immediate propagation
480 of deglacial environmental change to deep-marine turbidite systems along the Chile convergent margin:
481 *Earth and Planetary Science Letters*, v. 473, p. 190–204, doi: 10.1016/j.epsl.2017.05.017.
- 482 **Bolla Pittaluga, M. and Imran, J.**, 2014, A simple model for vertical profiles of velocity and suspended sediment
483 concentration in straight and curved submarine channels: *Journal of Geophysical Research*, v. 119, p. 483–
484 503, doi: 10.1002/(ISSN)2169-9011.
- 485 **Bondevik, S., Svendsen, J.I., Johnsen, G., Mangerud, J. and Kaland, P.E.**, 1997, The Storegga tsunami along the
486 Norwegian coast: Its age and run-up: *Boreas*, v. 26, p. 29–53, doi:10.1111/j.1502-3885.1997.tb00649.x.
- 487 **Bouma, A.H., Normark, W.R. and Barnes, N.E.**, 1985, *Submarine Fans and Related Turbidite Systems*: New
488 York, Springer-Verlag, 351 p.
- 489 **Burdige, D.J.**, 2005, Burial of terrestrial organic matter in marine sediments: A re-assessment: *Global*

- 490 Biogeochemical Cycles, v. 19, GB4011, p. 1-7, doi: 10.1029/2004GB002368.
- 491 **Calvès, G., Toucanne, S., Jouet, G., Charrier, S., Thereau, E., Etoubleau, J., Marsset, T., Droz, L., Bez, M.,**
492 **Abreu, V., Jorry, S., Mulder, T. and Lericolais, G.,** 2012, Inferring denudation variations from the
493 sediment record; an example of the last glacial cycle record of the Golo Basin and watershed, East Corsica,
494 western Mediterranean sea: Basin Research, v. 25, p. 197–218, doi: 10.1111/j.1365-2117.2012.00556.x.
- 495 **Carter, L., Milliman, J.D., Talling, P.J., Gavey, R. and Wynn, R.B.,** 2012, Near-synchronous and delayed
496 initiation of long run-out submarine sediment flows from a record-breaking river flood, offshore Taiwan:
497 Geophysical Research Letters, v. 39, 5 p., doi: 10.1029/2012GL051172.
- 498 **Cartigny, M.J.B., Eggenhuisen, J.T., Hansen, E.W.M. and Postma, G.,** 2013, Concentration-Dependent Flow
499 Stratification In Experimental High-Density Turbidity Currents and Their Relevance To Turbidite Facies
500 Models: Journal of Sedimentary Research, v. 83, p. 1046–1064, doi: 10.2110/jsr.2013.71.
- 501 **Castelltort, S., Honegger, L., Adatte, T., Clark, J.D., Puigdefàbregas, C., Spangenberg, J.E., Dykstra, M.L.**
502 **and Fildani, A.,** 2017, Detecting eustatic and tectonic signals with carbon isotopes in deep-marine strata,
503 Eocene Ainsa Basin, Spanish Pyrenees: Geology, p. G39068.1, doi: 10.1130/G39068.1.
- 504 **Clare, M.A., Talling, P.J., Challenor, P., Malgesini, G. and Hunt, J.,** 2014, Distal turbidites reveal a common
505 distribution for large (>0.1 km³) submarine landslide recurrence: Geology, v. 42, p. 263–266, doi:
506 10.1130/G35160.1.
- 507 **Clare, M.A., Talling, P.J. and Hunt, J.E.,** 2015, Implications of reduced turbidity current and landslide activity for
508 the Initial Eocene Thermal Maximum – evidence from two distal, deep-water sites: Earth and Planetary
509 Science Letters, v. 420, p. 102–115, doi: 10.1016/j.epsl.2015.03.022.
- 510 **Clare, M.A., Clarke, J.E.H., Talling, P.J., Cartigny, M.J.B. and Pratomo, D.G.,** 2016, Preconditioning and
511 triggering of offshore slope failures and turbidity currents revealed by most detailed monitoring yet at a
512 fjord-head delta: Earth and Planetary Science Letters, v. 450, p. 208–220, doi: 10.1016/j.epsl.2016.06.021.
- 513 **Clift, P.D.,** 2006, Controls on the erosion of Cenozoic Asia and the flux of clastic sediment to the ocean: Earth and
514 Planetary Science Letters, v. 241, p. 571–580, doi: 10.1016/j.epsl.2005.11.028.
- 515 **Cooper, C., Wood, J. and Andrieux, O.,** 2013, Turbidity current measurements in the Congo Canyon: Offshore
516 Technology Conference OTC-23992-MS, doi:10.4043/23992-MS.
- 517 **Croguennec, C., Ruffine, L., Dennielou, B., Baudin, F., Caprais, J.-C., Guyader, V., Bayon, G., Brandily, C.,**
518 **Le Bruchec, J., Bollinger, C., Germain, Y., Droz, L., Babonneau, N. and Rabouille, C.,** 2017, Evidence
519 and age estimation of mass wasting at the distal lobe of the Congo deep-sea fan: Deep-Sea Research Part II,

- 520 v. 142, p. 50–63, doi: 10.1016/j.dsr2.2016.12.013.
- 521 **de Leeuw, J., Eggenhuisen, J.T. and Cartigny, M.J.B.**, 2016, Morphodynamics of submarine channel inception
522 revealed by new experimental approach: *Nature Communications*, v. 7, p. 1-7, doi: 10.1038/ncomms10886.
- 523 **Denniellou, B., Droz, L., Babonneau, N., Jacq, C., Bonnel, C., Picot, M., Le Saout, M., Saout, Y., Bez, M.,**
524 **Savoie, B., Olu, K. and Rabouille, C.**, 2017, Morphology, structure, composition and build-up processes
525 of the active channel-mouth lobe complex of the Congo deep-sea fan with inputs from remotely operated
526 underwater vehicle (ROV) multibeam and video surveys: *Deep-Sea Research Part II*, v. 142, p. 25–49, doi:
527 10.1016/j.dsr2.2017.03.010.
- 528 **Deptuck, M.E., Piper, D.J.W., Savoie, B. and Gervais, A.**, 2008, Dimensions and architecture of late Pleistocene
529 submarine lobes off the northern margin of East Corsica: *Sedimentology*, v. 55, p. 869–898, doi:
530 10.1111/j.1365-3091.2007.00926.x.
- 531 **Dill, R.F., Dietz, R.S. and Stewart, H.**, 1954, Deep-Sea Channels and Delta of the Monterey Submarine Canyon:
532 *Geological Society of America Bulletin*, v. 65, p. 191–194, doi: 10.1130/0016-
533 7606(1954)65[191:DCADOT]2.0.CO;2.
- 534 **Fernandez, R.L., Cantelli, A., Pirmez, C., Sequeiros, O. and Parker, G.**, 2014, Growth Patterns of Subaqueous
535 Depositional Channel Lobe Systems Developed Over A Basement With A Downdip Break In Slope:
536 *Laboratory Experiments: Journal of Sedimentary Research*, v. 84, p. 168–182, doi: 10.2110/jsr.2014.10.
- 537 **Fildani, A., Weislogel, A., Drinkwater, N.J., McHargue, T., Tankard, A., Wooden, J., Hodgson, D. and Flint,**
538 **S.**, 2009, U-Pb zircon ages from the southwestern Karoo Basin, South Africa--Implications for the
539 Permian-Triassic boundary: *Geology*, v. 37, p. 719–722, doi: 10.1130/G25685A.1.
- 540 **Gervais, A.**, 2002, Analyse multi-échelles de la morphologie, de la géométrie et de l'architecture d'un système
541 turbiditique sableux profond (Système du Golo, Marge est Corse, Mer Méditerranée). Ph.D. Thesis,
542 University of Bordeaux I, no. 2621.
- 543 **Gervais, A., Mulder, T., Savoie, B. and Gonthier, E.**, 2006, Sediment distribution and evolution of sedimentary
544 processes in a small sandy turbidite system (Golo system, Mediterranean Sea): implications for various
545 geometries based on core framework: *Geo-Marine Letters*, v. 26, p. 373–395, doi: 10.1007/s00367-006-
546 0045-z.
- 547 **Goldfinger, C.**, 2011, Submarine Paleoseismology Based on Turbidite Records: *Annual Review of Marine Science*,
548 v. 3, p. 35–66, doi: 10.1146/annurev-marine-120709-142852.
- 549 **Gonzalez-Yajimovich, O.E., Gorsline, D.S. and Douglas, R.G.**, 2007, Frequency and sources of basin floor

- 550 turbidites in Alfonso basin, Gulf of California, Mexico: Products of slope failures: *Sedimentary Geology*, v.
551 199, p. 91–105, doi: 10.1016/j.sedgeo.2005.09.025.
- 552 **Gorsline, D.S.**, 1996, Depositional events in Santa Monica Basin, California Borderland, over the past five
553 centuries: *Sedimentary Geology*, v. 104, p. 73–88.
- 554 **Gulick, S.P.S., Jaeger, J.M., Mix, A.C., Asahi, H., Bahlburg, H., Belanger, C.L., Berbel, G.B.B., Childress, L.,**
555 **Cowan, E., Drab, L., Forwick, M., Fukumura, A., Ge, S., Gupta, S., et al.**, 2015, Mid-Pleistocene
556 climate transition drives net mass loss from rapidly uplifting St. Elias Mountains, Alaska: *Proceedings of*
557 *the National Academy of Sciences*, v. 112, p. 15042–15047, doi: 10.1073/pnas.1512549112.
- 558 **Hafliðason, H., Sejrup, H.P., Nygård, A., Mienert, J., Bryn, P., Lien, R., Forsberg, C.F., Berg, K. and Masson,**
559 **D.**, 2004, The Storegga Slide: architecture, geometry and slide development: *Marine Geology*, v. 213, p.
560 201–234, doi: 10.1016/j.margeo.2004.10.007.
- 561 **Heezen, B.C., Tharp, M. and Ewing, M.**, 1959, The Floors of the Oceans I. The North Atlantic, *In* Heezen, B.C.,
562 Tharp, M., and Ewing, M. eds., *The Floors of the Oceans: I. The North Atlantic*, Geological Society of
563 America Special Paper 65, doi: 10.1130/SPE65-p1.
- 564 **Hodgson, D.M., Flint, S.S., Hodgetts, D., Drinkwater, N.J., Johannessen, E.P. and Luthi, S.M.**, 2006,
565 Stratigraphic Evolution of Fine-Grained Submarine Fan Systems, Tanqua Depocenter, Karoo Basin, South
566 Africa: *Journal of Sedimentary Research*, v. 76, p. 20–40, doi: 10.2110/jsr.2006.03.
- 567 **Hubbard, S.M., Covault, J.A., Fildani, A. and Romans, B.W.**, 2014, Sediment transfer and deposition in slope
568 channels: Deciphering the record of enigmatic deep-sea processes from outcrop: *Geological Society of*
569 *America Bulletin*, v. 126, p. 857–871, doi: 10.1130/B30996.1.
- 570 **Hughes-Clarke, J.E.**, 2016, First wide-angle view of channelized turbidity currents links migrating cyclic steps to
571 flow characteristics: *Nature Communications*, v. 7, p. 1–13, doi: 10.1038/ncomms11896.
- 572 **Hunt, J.E., Wynn, R.B., Talling, P.J. and Masson, D.G.**, 2013, Frequency and timing of landslide-triggered
573 turbidity currents within the Agadir Basin, offshore NW Africa: Are there associations with climate
574 change, sea level change and slope sedimentation rates?: *Marine Geology*, v. 346, p. 274–291, doi:
575 10.1016/j.margeo.2013.09.004.
- 576 **Jegou, I., Savoye, B., Pirmez, C. and Droz, L.**, 2008, Channel-mouth lobe complex of the recent Amazon Fan: The
577 missing piece: *Marine Geology*, v. 252, p. 62–77, doi: 10.1016/j.margeo.2008.03.004.
- 578 **Jobe, Z.R., Sylvester, Z., Howes, N., Pirmez, C., Parker, A., Cantelli, A., Smith, R., Wolinsky, M.A., O’Byrne,**
579 **C., Slowey, N. and Prather, B.**, 2016, High-resolution, millennial-scale patterns of bed compensation on a

- 580 sand-rich intraslope submarine fan, western Niger Delta slope: Geological Society of America Bulletin, v.
581 129, p. 23–37, doi: 10.1130/B31440.1.
- 582 **Jobe, Z.R., Sylvester, Z., Bolla Pittaluga, M., Frascati, A., Pirmez, C., Minisini, D., Howes, N. and Cantelli, A.,**
583 2017, Facies architecture of submarine channel deposits on the western Niger Delta slope: Implications for
584 grain-size and density stratification in turbidity currents: Journal of Geophysical Research: Earth Surface,
585 v. 122, p. 473–491, doi: 10.1002/2016JF003903.
- 586 **Kane, I.A. and Ponten, A.S.M.,** 2012, Submarine transitional flow deposits in the Paleogene Gulf of Mexico:
587 Geology, v. 40, p. 1119–1122, doi: 10.1130/G33410.1.
- 588 **Kolla, V. and Perlmutter, M.A.,** 1993, Timing of Turbidite Sedimentation on the Mississippi Fan: AAPG Bulletin,
589 v. 77, p. 1129–1141.
- 590 **Lamb, M.P., Hickson, T., Marr, J.G., Sheets, B. and Paola, C.,** 2004, Surging versus continuous turbidity
591 currents: flow dynamics and deposits in an experimental intraslope minibasin: Journal of Sedimentary
592 Research, v. 74, p. 148–155.
- 593 **Mallarino, G., Beaubouef, R.T., Droxler, A.W., Abreu, V. and Labeyrie, L.,** 2006, Sea level influence on the
594 nature and timing of a minibasin sedimentary fill (northwestern slope of the Gulf of Mexico): AAPG
595 Bulletin, v. 90, p. 1089–1119, doi: 10.1306/02210605058.
- 596 **McHargue, T., Pyrcz, M.J., Sullivan, M.D., Clark, J.D., Fildani, A., Romans, B.W., Covault, J.A., Levy, M.,**
597 **Posamentier, H.W. and Drinkwater, N.J.,** 2011, Architecture of turbidite channel systems on the
598 continental slope: Patterns and predictions: Marine and Petroleum Geology, v. 28, p. 728–743, doi:
599 10.1016/j.marpetgeo.2010.07.008.
- 600 **McKay, M.P., Weislogel, A.L., Fildani, A., Brunt, R.L., Hodgson, D.M. and Flint, S.S.,** 2015, U-PB zircon tuff
601 geochronology from the Karoo Basin, South Africa: implications of zircon recycling on stratigraphic age
602 controls: International geology review, v. 57, p. 393–410, doi: 10.1080/00206814.2015.1008592.
- 603 **Menard, H.W.,** 1955, Matching Land and Sea Floor Topography and Structures off California: AAPG Bulletin, v.
604 39, p. 137–137.
- 605 **Milliman, J.D. and Farnsworth, K.L.,** 2011, River Discharge to the Coastal Ocean: A Global Synthesis.
606 Cambridge University Press, Cambridge, 384 p.
- 607 **Murray, C.J., Lowe, D.R. and Graham, S.A.,** 1996, Statistical analysis of bed-thickness patterns in a turbidite
608 section from the Great Valley Sequence, Cache Creek, Northern California: Journal of Sedimentary
609 Research, v. 66, p. 900–908.

- 610 **Mutti, E. and Normark, W.R.**, 1987, Comparing Examples of Modern and Ancient Turbidite Systems: Problems
611 and Concepts, in *Marine Clastic Sedimentology*, Dordrecht, Springer, Dordrecht, p. 1–38.
- 612 **Normark, W.R.**, 1970, Growth Patterns of Deep-Sea Fans: *AAPG Bulletin*, v. 54, p. 2170–2195.
- 613 **Normark, W.R., and Piper, D.J.W.**, 1991, Initiation processes and flow evolution of turbidity currents:
614 implications for the depositional record. *SEPM Special Publication no. 46 “From Shoreline to Abyss”*, p.
615 207-230.
- 616 **Normark, W.R., Piper, D. and Hiscott, R.N.**, 1998, Sea level controls on the textural characteristics and
617 depositional architecture of the Hueneme and associated submarine fan systems, Santa Monica Basin,
618 California: *Sedimentology*, v. 45, p. 53–70.
- 619 **Normark, W.R., Piper, D.J.W. and Sliter, R.**, 2006, Sea-level and tectonic control of middle to late Pleistocene
620 turbidite systems in Santa Monica Basin, offshore California: *Sedimentology*, v. 53, p. 867–897, doi:
621 10.1111/j.1365-3091.2006.00797.x.
- 622 **Paola, C. and Voller, V.R.**, 2005, A generalized Exner equation for sediment mass balance, *J. Geophys. Res.*, v.
623 110, F04014, doi:10.1029/2004JF000274.
- 624 **Paull, C.K., Mitts, P., Ussler, W., Keaten, R., and Greene, H.G.**, 2005, Trail of sand in upper Monterey Canyon:
625 Offshore California: *Geological Society of America Bulletin*, v. 117, p. 1134, doi: 10.1130/B25390.1.
- 626 **Paull, C.K., Ussler, W., III, Caress, D.W., Lundsten, E., Covault, J.A., Maier, K.L., Xu, J. and Augenstein, S.**,
627 2010, Origins of large crescent-shaped bedforms within the axial channel of Monterey Canyon, offshore
628 California: *Geosphere*, v. 6, p. 755–774, doi: 10.1130/GES00527.1.
- 629 **Paull, C.K., McGann, M., Sumner, E.J., Barnes, P.M., Lundsten, E.M., Anderson, K., Gwiazda, R., Edwards,**
630 **B. and Caress, D.W.**, 2014, Sub-decadal turbidite frequency during the early Holocene: Eel Fan, offshore
631 northern California: *Geology*, v. 42, p. 855–858, doi: 10.1130/G35768.1.
- 632 **Petit, C., Migeon, S. and Coste, M.**, 2015, Numerical models of continental and submarine erosion: application to
633 the northern Ligurian Margin (Southern Alps, France/Italy): *Earth Surface Processes and Landforms*, v. 40,
634 p. 681–695, doi: 10.1002/esp.3685.
- 635 **Pettingill, H.S. and Weimer, P.**, 2002, Worldwide deepwater exploration and production: Past, present, and future:
636 *The Leading Edge*, v. 21, p. 371–376, doi: 10.1190/1.1471600.
- 637 **Picot, M., Droz, L., Marsset, T., Dennielou, B. and Bez, M.**, 2016, Controls on turbidite sedimentation: Insights
638 from a quantitative approach of submarine channel and lobe architecture (Late Quaternary Congo Fan):
639 *Marine and Petroleum Geology*, v. 72, p. 423–446, doi: 10.1016/j.marpetgeo.2016.02.004.

- 640 **Piper, D. and Aksu, A.E.**, 1987, The Source and Origin of the 1929 Grand Banks Turbidity Current Inferred from
641 Sediment Budgets: *Geo-Marine Letters*, v. 7, p. 177–182, doi: 10.1007/BF02242769.
- 642 **Piper, D. and Normark, W.R.**, 1983, Turbidite Depositional Patterns and Flow Characteristics, Navy Submarine
643 Fan, California Borderland: *Sedimentology*, v. 30, p. 681–694, doi: 10.1111/j.1365-3091.1983.tb00702.x.
- 644 **Piper, D. and Normark, W.R.**, 2001, Sandy fans--from Amazon to Hueneme and beyond: *AAPG Bulletin*, v. 85, p.
645 1407–1438.
- 646 **Piper, D.J.W.**, and **Normark, W.R.**, 2009, Processes That Initiate Turbidity Currents and Their Influence on
647 Turbidites: A Marine Geology Perspective: *Journal of Sedimentary Research*, v. 79, p. 347–362, doi:
648 10.2110/jsr.2009.046.
- 649 **Pirmez, C., Hiscott, R.N. and Kronen, J.**, 1997, Sandy turbidite successions at the base of channel-levee systems
650 on the Amazon Fan: unraveling the facies architecture of large submarine fans: *Proceedings of the Ocean*
651 *Drilling Program. Scientific Results*, vol. 155, p. 7-33.
- 652 **Pirmez, C., Beaubouef, R.T., Friedmann, S.J. and Mohrig, D.C.**, 2000, Equilibrium profile and base level in
653 submarine channels: examples from Late Pleistocene systems and implications for the architecture of
654 deepwater reservoirs: in *Gulf Coast Section SEPM Foundation 20th Annual Bob F. Perkins Research*
655 *Conference, Global Deep-Water Reservoirs*, p. 782-805, doi: 10.5724/gcs.12.32.
- 656 **Pirmez, C., Prather, B.E., Mallarino, G. and O'Hayer, W.W.**, 2012, Chronostratigraphy of the Brazos–Trinity
657 depositional System, Western Gulf of Mexico: implications for deepwater depositional models: *Application*
658 *of the Principles*
- 659 **Prather, B.E., Pirmez, C. and Winker, C.D.**, 2012b Stratigraphy of linked intraslope basins: Brazos–Trinity
660 system western Gulf of Mexico: *in* Prather, B.E., Deptuck, M.E., Mohrig, D., van Hoorn, B., and Wynn, R.,
661 eds., *Application of the Principles of Seismic Geomorphology to Continental-Slope and Base-of-Slope*
662 *Systems: Case Studies from Seafloor and Near-Seafloor Analogues: Society for Sedimentary Geology*
663 *(SEPM) Special Publication 99*, p. 83-109.
- 664 **Prather, B.E., Pirmez, C., Sylvester, Z. and Prather, D.S.**, 2012a Stratigraphic response to evolving
665 geomorphology in a submarine apron perched on the upper Niger Delta slope: *in* Prather, B.E., Deptuck,
666 M.E., Mohrig, D., van Hoorn, B., and Wynn, R., eds., *Application of the Principles of Seismic*
667 *Geomorphology to Continental-Slope and Base-of-Slope Systems: Case Studies from Seafloor and Near-*
668 *Seafloor Analogues: Society for Sedimentary Geology (SEPM) Special Publication 99*, p. 347-369.
- 669 **Prélat, A. and Hodgson, D.M.**, 2013, The full range of turbidite bed thickness patterns in submarine lobes: controls
670 and implications: *Journal of the Geological Society*, v. 170, p. 209–214, doi: 10.1144/jgs2012-056.

- 671 **Prélat, A., Hodgson, D.M. and Flint, S.S.,** 2009, Evolution, architecture and hierarchy of distributary deep-water
672 deposits: a high-resolution outcrop investigation from the Permian Karoo Basin, South Africa:
673 *Sedimentology*, v. 56, p. 2132–2154, doi: 10.1111/j.1365-3091.2009.01073.x.
- 674 **Prélat, A., Covault, J.A., Hodgson, D.M., Fildani, A. and Flint, S.S.,** 2010, Intrinsic controls on the range of
675 volumes, morphologies, and dimensions of submarine lobes: *Sedimentary Geology*, v. 232, p. 66–76, doi:
676 10.1016/j.sedgeo.2010.09.010.
- 677 **Prior, D.B., Bornhold, B.D., Wiseman, W.J. and Lowe, D.R.,** 1987, Turbidity Current Activity in a British
678 Columbia Fjord: *Science*, v. 237, p. 1330–1333, doi: 10.1126/science.237.4820.1330.
- 679 **Pyles, D.R.,** 2008, Multiscale stratigraphic analysis of a structurally confined submarine fan: Carboniferous Ross
680 Sandstone, Ireland: *AAPG Bulletin*, v. 92, p. 557–587, doi: 10.1306/01110807042.
- 681 **Romans, B.W., Normark, W.R., McGann, M.M., Covault, J.A. and Graham, S.A.,** 2009, Coarse-grained
682 sediment delivery and distribution in the Holocene Santa Monica Basin, California: Implications for
683 evaluating source-to-sink flux at millennial time scales: *Geological Society of America Bulletin*, v. 121, p.
684 1394–1408, doi: 10.1130/B26393.1.
- 685 **Romans, B.W., Castellort, S., Covault, J.A., Fildani, A. and Walsh, J.P.,** 2016, Environmental signal
686 propagation in sedimentary systems across timescales: *Earth Science Reviews*, v. 153, p. 7–29, doi:
687 10.1016/j.earscirev.2015.07.012.
- 688 **Saller, A., Werner, K., Sugiaman, F., Cebastian, A., May, R., Glenn, D. and Barker, C.,** 2008, Characteristics
689 of Pleistocene deep-water fan lobes and their application to an upper Miocene reservoir model, offshore
690 East Kalimantan, Indonesia: *AAPG Bulletin*, v. 92, p. 919–949, doi: 10.1306/03310807110.
- 691 **Sequeiros, O.E., Spinewine, B. and Beaubouef, R.T.,** 2010, Characteristics of velocity and excess density profiles
692 of saline underflows and turbidity currents flowing over a mobile bed: *Journal of Hydraulic Engineering*, v.
693 10.1061/(ASCE)HY.1943-7900.0000200, p. 412–433, doi: 10.1061/ ASCE HY.1943-7900.0000200.
- 694 **Shepard, F.P. and Emery, K.O.,** 1941, Submarine Topography off the California Coast: Canyons and Tectonic
695 Interpretations: *Geological Society of America Special Paper* 31, doi: 10.1130/SPE31.
- 696 **Sømme, T.O., Helland-Hansen, W., Martinsen, O.J., and Thurmond, J.B.,** 2009, Relationships between
697 morphological and sedimentological parameters in source-to-sink systems: a basis for predicting semi-
698 quantitative characteristics in subsurface systems: *Basin Research*, v. 21, p. 361–387, doi: 10.1111/j.1365-
699 2117.2009.00397.x.
- 700 **Sømme, T.O., Piper, D.J.W., Deptuck, M.E. and Helland-Hansen, W.,** 2011, Linking Onshore-Offshore

- 701 Sediment Dispersal in the Golo Source-to-Sink System (Corsica, France) During the Late Quaternary:
702 Journal of Sedimentary Research, v. 81, p. 118–137, doi: 10.2110/jsr.2011.11.
- 703 **Spinewine, B., Sequeiros, O.E., Garcia, M.H., Beaubouef, R.T., Sun, T., Savoye, B. and Parker, G.,** 2009,
704 Experiments on Wedge-Shaped Deep Sea Sedimentary Deposits in Minibasins and/or on Channel Levees
705 Emplaced by Turbidity Currents. Part II. Morphodynamic Evolution of the Wedge and of the Associated
706 Bedforms: Journal of Sedimentary Research, v. 79, p. 608–628, doi: 10.2110/jsr.2009.065.
- 707 **Stevens, T., Paull, C.K., Ussler, W., McGann, M., Buylaert, J.P. and Lundsten, E.,** 2013, The timing of
708 sediment transport down Monterey Submarine Canyon, offshore California: Geological Society of America
709 Bulletin, v. 126, p. 103–121, doi: 10.1130/B30931.1.
- 710 **Stevenson, C.J., Jackson, C.A.L., Hodgson, D.M., Hubbard, S.M. and Eggenhuisen, J.T.,** 2015, Deep-Water
711 Sediment Bypass: Journal of Sedimentary Research, v. 85, p. 1058–1081, doi: 10.2110/jsr.2015.63.
- 712 **Sylvester, Z.,** 2007, Turbidite bed thickness distributions: methods and pitfalls of analysis and modelling:
713 Sedimentology, v. 54, p. 847–870, doi: 10.1111/j.1365-3091.2007.00863.x.
- 714 **Sylvester, Z., Cantelli, A. and Pirmez, C.,** 2015, Stratigraphic evolution of intraslope minibasins: Insights from
715 surface-based model: AAPG Bulletin, v. 99, p. 1099–1129, doi: 10.1306/01081514082.
- 716 **Symons, W.O., Sumner, E.J., Paull, C.K., Cartigny, M.J.B., Xu, J.P., Maier, K.L., Lorenson, T.D. and Talling,**
717 **P.J.,** 2017, A new model for turbidity current behavior based on integration of flow monitoring and
718 precision coring in a submarine canyon: Geology, v. 45, p. 367–370, doi: 10.1130/G38764.1.
- 719 **Talling, P.J.,** 2001, On the frequency distribution of turbidite thickness: Sedimentology, v. 48, p. 1297–1329.
- 720 **Talling, P.J., Amy, L.A. and Wynn, R.B.,** 2007a, New insight into the evolution of large-volume turbidity currents:
721 comparison of turbidite shape and previous modelling results: Sedimentology, v. 54, p. 737–769, doi:
722 10.1111/j.1365-3091.2007.00858.x.
- 723 **Talling, P.J., Wynn, R.B., Masson, D.G., Frenz, M., Cronin, B.T., Schiebel, R., Akhmetzhanov, A.M.,**
724 **Dallmeier-Tiessen, S., Benetti, S., Weaver, P.P.E., Georgiopoulou, A., Zühlendorff, C. and Amy, L.A.,**
725 2007b, Onset of submarine debris flow deposition far from original giant landslide: Nature, v. 450, p. 541–
726 544, doi: 10.1038/nature06313.
- 727 **Talling, P.J., Allin, J., Armitage, D.A., Arnott, R.W.C., Cartigny, M.J.B., Clare, M.A., Felletti, F., Covault,**
728 **J.A., Girardclos, S., Hansen, E., Hill, P.R., Hiscott, R.N., Hogg, A.J., Hughes-Clarke, J., Jobe, Z.R., et**
729 **al.,** 2015, Key Future Directions for Research On Turbidity Currents and Their Deposits: Journal of
730 Sedimentary Research, v. 85, p. 153–169, doi: 10.2110/jsr.2015.03.

- 731 **Walker, R.G.**, 1978, Deep-water sandstone facies and ancient submarine fans: models for exploration for
732 stratigraphic traps: AAPG Bulletin, v. 62, p. 932–966.
- 733 **Weaver, P., Rothwell, R.G., Ebbing, J., Gunn, D. and Hunter, P.M.**, 1992, Correlation, Frequency of
734 Emplacement and Source Directions of Megaturbidites on the Madeira Abyssal-Plain: Marine Geology, v.
735 109, p. 1–20, doi: 10.1016/0025-3227(92)90218-7.
- 736 **Wilson, C.A. and Goodbred, S.L., Jr.**, 2015, Construction and Maintenance of the Ganges-Brahmaputra-Meghna
737 Delta: Linking Process, Morphology, and Stratigraphy: Annual Review of Marine Science, v. 7, p. 67–88,
738 doi: 10.1146/annurev-marine-010213-135032.
- 739 **Winker, C.D.**, 1996, High-Resolution Seismic Stratigraphy of a Late Pleistocene Submarine Fan Ponded by Salt-
740 Withdrawal Mini-Basins on the Gulf of Mexico Continental Slope. Offshore Technology Conference OTC-
741 8024-MS. doi:10.4043/8024-MS.
- 742 **Xu, J.P., Sequieros, O.E. and Noble, M.A.**, 2014, Sediment concentrations, flow conditions, and downstream
743 evolution of two turbidity currents, Monterey Canyon, USA: Deep-Sea Research Part I, v. 89, p. 11–34,
744 doi: 10.1016/j.dsr.2014.04.001.
- 745

746

747

Study area ^(refs.)	Tectonic regime	Slope/Basin Position	Water depth (m)	Distance from shelf edge (km)	Age range (ka)
Niger X system, Nigeria ^{(1), (2), (3)}	Passive margin with shale tectonics	Intraslope, not ponded	1200	61	25-15
Hueneme system California ^{(4), (5)}	Active; Flexural transpressional basin with fault-controlled basin margins	Basin floor and ponded	850	30	7-0
Golo system, Corsica ^{(6), (7), (8)}	Active margin with fault-controlled basin topography	Basin floor, not ponded	800	20	57-15 (5); 130-0 (6)
		Intraslope, not ponded	800	20	25-18 (6)
Brazos-Trinity system, Gulf of Mexico ^{(9), (10)}	Passive margin with salt tectonics and ponded mini-basin formation	Intraslope, ponded	900 (Basin II); 1500 (Basin IV)	40 (Basin II); 75 (Basin IV)	23-15 (all basins)

748

749 Table 1. Characteristics of the locales utilized in this study. References cited include: (1) Jobe *et*
750 *al.* (2016); (2) Milliman and Farnsworth (2011); (3) Allen (1965); (4) Romans *et al.* (2009); (5)
751 Gorsline (1996); (6) Gervais *et al.* (2006); (7) Sømme *et al.* (2011); (8) Calves *et al.* (2012); (9)
752 Pirmez *et al.* (2012); (10) Prather *et al.* (2012b).

753

754

Locale		Bulk volume (m ³)	Porosity	Sediment volume V (m ³) (porosity subtracted)	total time T (years)	n (event bed count)	Catchment Area (km ²)	Sediment Yield (tons/km ² /yr)	Sediment Load (Megatons/yr)
Niger X	data (min; max)	1.72x10 ⁷ ; 5.16x10 ⁷	0.4	1.20x10 ⁷ ; 3.61x10 ⁷	3800; 4400	48; 20	5.50x10 ⁵	4.55	2.5
	notes	using area and 1-3 m thickness from (1)	from multi-sensor core logger data (1)	calculated from bulk volume by subtracting porosity	Fig. 9 of (1)	bend 5; fan 14 cores of (1)	These values represent one-fourth of the Niger River values from (2), as one-fourth of sediment discharge is distributed to the X fan area (3)		
Hueneme Interval 1	data (min; max)	4.58 x 10 ⁹	0.38	2.84 x 10 ⁹	2700; 2800	7; 9	5420	2712	14.7
	notes	Table 3 of (4)	Page 1399 of (4)	Table 3 of (4)	Table 3 of (4)	Table 2, Fig 3 of (4)			
Hueneme Interval 2	data (min; max)	3.57 x 10 ⁹	0.38	2.21 x 10 ⁹	2340; 2440	6; 8			
	notes	Table 3 of (4)	Page 1399 of (4)	Table 3 of (4)	Table 3 of (4)	Table 2, Fig 3 of (4)			
Hueneme Intervals 3,4,5	data (min; max)	6.12 x 10 ⁹	0.38	3.80 x 10 ⁹	500; 1760	4; 7	Summed values of Santa Clara River, Ventura River, and Calleguas Creek from (2)		
	notes	Table 3 of (4)	Page 1399 of (4)	Table 3 of (4)	Value from (5); Fig. 3 of (4)	Value from (5); Fig. 3 of (4)			
Golo Somme	data (min; max)	Bulk volume to sediment volume performed by (7)		4.04 x 10 ⁹	14000;16000	68; 136	1214 from (8)	2.2 from (2)	0.002 from (2)
	notes			Table 4 (seafloor to K) of (7)	Fig 7 of (7)	extrapolated from core data of (6)			
Golo Pineto	data (min; max)			3.12 x 10 ⁷ ; 3.55 x 10 ⁷	2444.5; 6222	12; 53			
	notes			Supp. Table 3 of (8)		extrapolated from core data of (6)			
Golo S1	data (min; max)			8.06 x 10 ⁸ ; 1.33 x 10 ¹⁰	68150; 90700	332; 772			
	notes	Bulk volume to sediment volume performed by (8)		Supp. Table 3 of (8)		extrapolated from core data of (6)			
Golo S2	data (min; max)			5.89 x 10 ⁷ ; 9.66 x 10 ⁹	22000; 29090	107; 248			
	notes			Supp. Table 3 of (8)		extrapolated from core data of (6)			
Golo S3	data (min; max)			1.06 x 10 ⁸ ; 1.91 x 10 ⁹	15860; 17100	77; 146			
	notes			Supp. Table 3 of (8)		extrapolated from core data of (6)			
Brazos Trinity 70 series	data (min; max)			2.72 x 10 ⁹	2000; 3000	10	1.94x10 ⁵	57.99	11.25
	notes			Fig 15 (all basins) of (9)	Table 2 and pg. 129 of (9)	Fig 4 of (9)			
Brazos Trinity 50/60 series	data (min; max)			1.85 x 10 ⁹	1100; 1500	12			
	notes	Bulk volume to sediment volume performed by (9)		Fig 15 (all basins) of (9)	Fig. 15 and pg. 129 of (9)	Fig 4 of (9)			
Brazos Trinity 40 series	data (min; max)			1.52 x 10 ⁹	2500; 3900	6	Summed values of Brazos, Trinity, and Sabine rivers from (2)		
	notes			Fig 15 (all basins) of (9)	Fig. 15 and pg. 129 of (9)	Fig 4 of (9)			

756

757 Table 2. Values of V , T , n , and other pertinent data for the four studied locales. See list of
 758 citations in Table 1 for data sources.

759

Skoorsteenberg Formation lobe deposits (Prelat et al., 2009)	Lobe volume V (m ³) from Prelat	event count n from Fig. 8 of Prelat	v_e (m ³) using Eqn. 2	Range of r (yr) from Fig. 5	Range of v_e (m ³) from Fig. 5	T (P ₁₀) estimate, yr	T (P ₅₀) estimate, yr	T (P ₉₀) estimate, yr
Lobe 2	2.2 x 10 ⁹	7	3.1 x 10 ⁸	50; 650	1.0x10 ⁷ ; 1.0x10 ⁹	446	1,526	7,260
lobe 5	3.5 x 10 ⁹	20	1.8 x 10 ⁸	50; 650	1.0x10 ⁷ ; 1.0x10 ⁹	745	2,486	11,339
lobe 6	1.3 x 10 ⁹	12	1.1 x 10 ⁸	50; 650	1.0x10 ⁷ ; 1.0x10 ⁹	273	900	4,332

760

761 Table 3. Values of parameters used to calculate total time of deposition (T) for submarine-fan
 762 deposits of the Skoorsteenberg Formation, South Africa.

763

764

765

766

767 Fig. 1. Framework for calculating event volume and recurrence interval of submarine-fan-
768 building turbidity currents, using three variables (V , T , n) from deposits. V = total sediment
769 volume, T = total duration of deposition, n = event count, r = recurrence interval, v_e = event
770 volume. Figure modified after Jobe *et al.* (2016).

771

772

773

774

775 Fig. 2. Map showing locations of late Quaternary submarine fan deposits analyzed in this study.

776

777

778

779

780

781 Fig. 3. Niger X fan seafloor depth map (10 m contours) with seismic amplitude (colour) and core
782 locations (white circles). Two cores used in the calculation of turbidity current recurrence are
783 shown at left and right. The black shaded region delineates the youngest sediment package of the
784 Niger X fan. Figure modified after Jobe *et al.* (2016).

785

786

787

788 Fig. 4. Size-recurrence plot for formative turbidity currents of the Niger X fan using (A) uniform
789 distributions of input values V , T , and n and (B) triangular distributions of input values V , T , and
790 n . Grey dots are the 10,000 iterations, and the dashed line is the convex hull of the uniformly
791 distributed data shown in part A. In (B), the black contour lines represent a 2D kernel density
792 contour map of 90% of the data, and the cross is the data centroid.

793

794

795

796 Fig. 5. Parameter-space for event volume (v_e) and recurrence interval (r) of Quaternary
797 submarine fan deposits. The convex hull is shown for each locale as calculated from uniformly
798 distributed variables. Event volume varies over four orders of magnitude while recurrence
799 interval only varies by one. Note that intraslope deposits tend to have lower event volumes than
800 deposits of base-of-slope and ponded systems (see discussion in text).

801

802

803

804 Fig. 6. Cumulative distribution of the estimated total time of deposition (T) for submarine-fan
805 deposits of the Permian Skoorsteenberg Formation, South Africa (nomenclature from Prélat *et*
806 *al.*, 2009). Vertical bars represent ranges of T for Late Quaternary Amazon and Zaire submarine-
807 fan deposits.

808

809

810

811

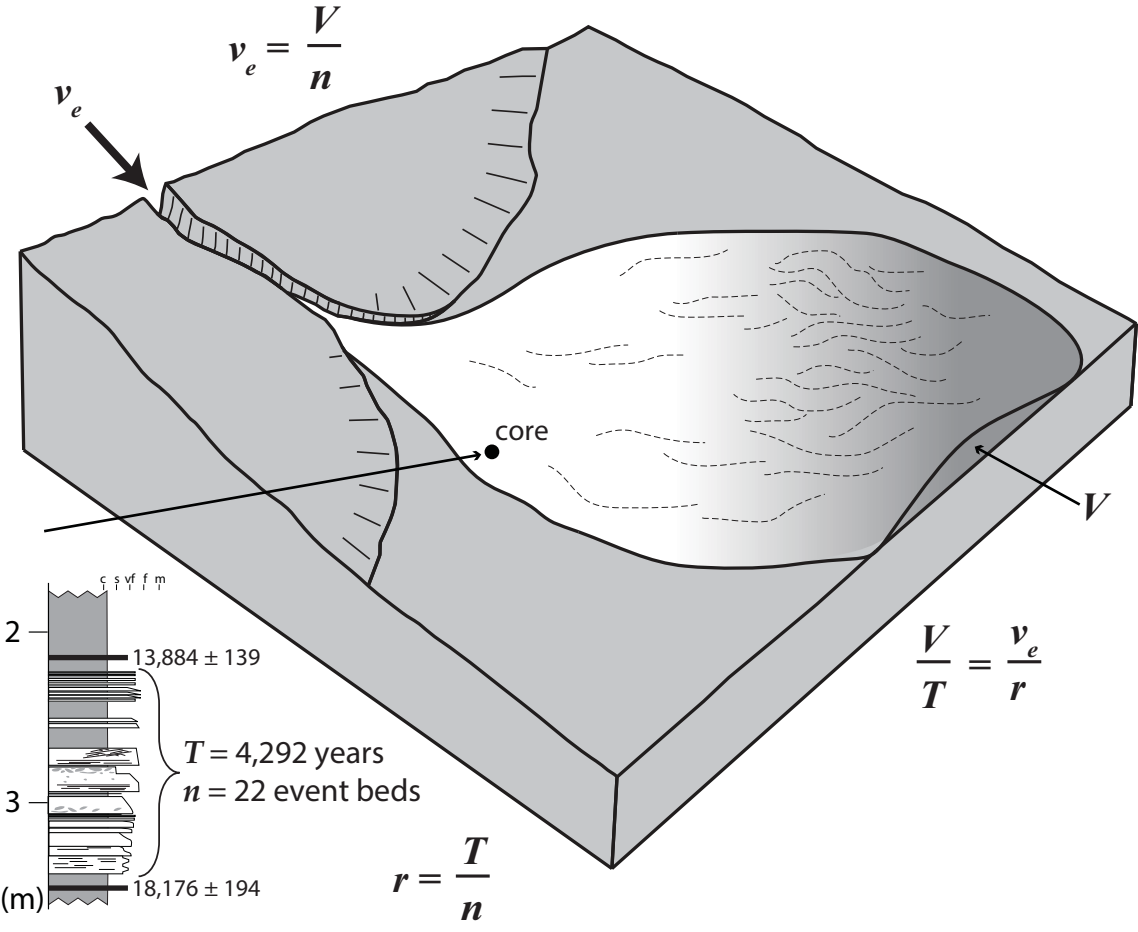
812 Fig. 7. Scaling relationships between median event volume and catchment parameters (A)
813 catchment area, (B) sediment yield, and (C) total sediment load. There is weak positive scaling
814 between median event volume and catchment parameters (dashed arrows), particularly sediment
815 yield. More systems need to be characterized to validate these scaling relationships. The Niger
816 forms a consistent outlier, suggesting that the sediment partitioning (Allen, 1965) is inaccurate.

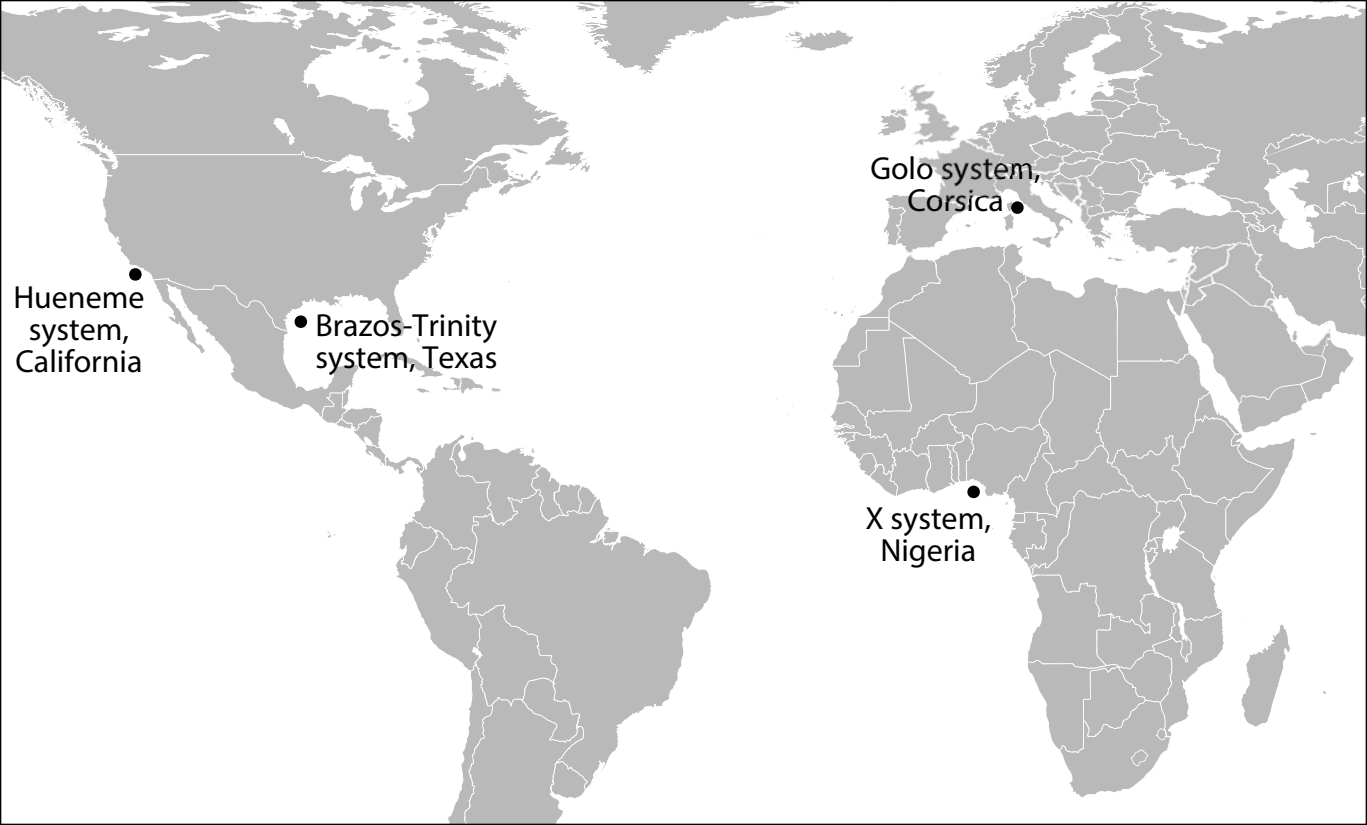
817

818

819 Fig. 8. Simplified parameter space for event volume and recurrence of turbidity currents across
820 the submarine sediment routing system (inspired by Piper & Normark, 1983). Frequent, small
821 volume flows begin in the canyon, but often do not reach the fan. Larger and less frequent flows
822 build submarine fans, but generally do not reach the abyssal plain. Only very rare, very large
823 flows reach the abyssal plain. The plot is overlain with a simplified submarine sediment routing
824 system for visualization purposes. Note the overlap between the largest scales calculated by this
825 study and that of abyssal plain turbidites, suggesting a continuum of flow properties between
826 submarine fans and abyssal plains.

827





Hueneme system,
California

• Brazos-Trinity
system, Texas

Golo system,
Corsica

X system,
Nigeria

